Low Mass Flux Upward Vertical Forced Flow Boiling of HFE7000

M. Eraghubi[1], P. Di Marco[2], A.J. Robinson[1]

[1]Department of Mechanical & Manufacturing Engineering, Parsons Building, Trinity College Dublin, Ireland.
[2]DESTEC, University of Pisa, Italy.

Abstract

Forced convective boiling experiments with HFE7000 as the working fluid were conducted for upward flow in a vertical tube at 122 kPa (1.2 bar), inlet subcooling of 2K and mass flux ranging between 50 and 150 kg/m²s. The experimental facility consisted of a smooth 8 mm inside diameter optically transparent sapphire tube with overall length of 120 mm. A central 80 mm long section was coated with optically transparent and electrically conductive Indium Tin Oxide (ITO) functioning as a heater to facilitate boiling whilst allowing for visual observation of the two-phase flow. Tests were performed by fixing the flow rate and progressively increasing the heat flux. The results show that after the onset of nucleate boiling, the flow regime is bubbly and increasing the heat flux acts to increase the boiling heat transfer coefficient due to increased nucleation site density, bubble frequency and size. This results in a linear increase in the boiling curve. However, once slug flow is established, the slope of the boiling curve increases indicating that this flow regime augments the heat transfer positively. Overall, the boiling curves were insensitive to mass flux for the range tested. However, the inflection on the boiling curve, associated with flow regime transition from bubbly to slug, was observed to be sensitive to mass flux. The Chen convective boiling heat transfer correlation was compared with the measured data showing reasonable agreement. A modified Chen correlation has been proposed for low mass flux convective boiling which predicts the measured data more accurately.

Keywords: Convective boiling; Two phase flow; Vertical upflow; Heat transfer; Flow regimes

1. Introduction

Flow boiling is a very effective engineering technology for removing large quantities of heat at targeted operational temperatures due to the large latent heat of vaporization associated with phase change and the high heat transfer coefficients compared with single-phase flow. The latent heat transfer also allows for relatively small inlet-to-outlet temperature differences compared to the single-phase flow [1].

The dominant heat transfer mechanisms during flow boiling depends on the flow regime, and is generally related to vaporization across thin liquid films, nucleate boiling or a combination of the two. At lower vapour qualities, the heat transfer coefficient depends strongly on the formation and departure of discrete bubbles from the heated wall. The periodic growth and release of bubbles agitates the thermal boundary layer at the wall which enhances the heat transfer over that of single phase flow. Increasing the heat flux results in increased vapour production which causes the boiling heat transfer to increase due to progressively increased agitation caused by the bubbles. At some point the vapour fraction is large enough that bubble coalescence increases to the point that vapour slugs form within the channel and the heat transfer is then a mix of nucleate boiling and conduction-convection-vaporization across liquid films between the wall and the slugs. Further increase in heat flux and vapour production rate causes the merging of slugs and a churn flow regime is established whereby the heat transfer is characterized by some nucleate boiling in combination with chaotic tossing, stirring and mixing of the two phases [2]. Increasing the heat flux, and thus vapour quality, even further results in the transition to annular flow which is characterized by an annular liquid film around the wall and a core of vapour and entrained liquid drops. Here the heat is transferred by conduction and convection across the film while evaporation takes place at the liquid-vapour interface. Here, the heat transfer coefficient is less dependent on the heat flux and tends to increase with the increase in mass velocity and vapour quality [3].

The complexity of diabatic two phase flows makes purely mechanistic models unsuitable for predicting the fluid mechanics and heat transfer. Although much progress has been made, direct numerical simulations of diabatic two phase flows of this type are also some time away. Historically then, the heat transfer during convective boiling has been predicted by empirical correlations. In the literature, dozens of correlations have

been published that aim to provide robust and accurate predictions of the convective boiling heat transfer over a wide range of fluid properties and operating conditions. Some of the more popular correlations are; Chen [4], Shah [5], Lazarek and Black [6], Gungor and Winterton [7,8], Kenning and Cooper [9], Kandlikar [10], Liu and Winterton [11], Wattelet [12], Sun and Mishima [13].

These listed correlations have approached the problem in different ways, both mathematically and from the standpoint of the base modelling strategy. However, one consistency across the correlations is that the heat transfer is assumed to be based on single phase convective heat transfer which is then augmented by two phase heat transfer related to the phase interactions of the vapour, liquid and solid. Typically, the correlations are developed by making a hypothesis regarding how the two-phase component augments the heat transfer and a model is structured around this hypothesis. The correlation is then developed by regression-fitting the model to a large data base of convective boiling measurements.

One problem with this approach is that the preponderance of the boiling data has been obtained in opaque metallic test sections where it is difficult to relate the heat transfer to the flow regime, and thus verify the efficacy of the underlying model. Another problem is that the models give markedly different predictions of the heat transfer for ostensibly the same operating conditions. Of course, this then becomes problematic when designing two-phase heat exchangers.

In this work, convective boiling is revisited. Here, the vertical upflow orientation is selected to avoid transverse gravitations effects which simplifies the flow patterns to some degree, in that it eliminates stratification at lower mass fluxes and generates more radially symmetric flow patterns. A transparent heated test section is utilized to gain some preliminary understanding of the local heat transfer and the flow regimes.

In this regard, the overarching objective of the present investigation is to contribute to the understanding of low quality and low mass flux vertical upflow convective boiling. To this end, local heat transfer measurements are analysed, and boiling heat transfer is investigated in the context of boiling curves. Specifically, the influence of mass and heat flux on vertical upward flow boiling are investigated and the results discussed in terms of the observed local flow regimes. Finally, the heat transfer coefficient results are compared with the well-assessed and widely used Chen [4] correlation and discussed in the context of the underlying modelling strategy. A straight forward modification of the Chen correlation is proposed for low mass flux convective boiling that improves agreement with the present measurements

2. Experimental apparatus and data reduction

The two-phase flow loop was designed and constructed to facilitate thermal and hydraulic measurements, including high speed videography, for a vertical tube with convective flow boiling occurring on its inner surface. The apparatus incorporates a transparent test section, which provides direct visual access to the flowing and boiling fluid. The test section is ohmically heated via a transparent yet electrically conductive ITO coating deposited on the outer surface of a sapphire tube. Importantly, sapphire has a thermal conductivity commensurate with some metals (~25 W/mK) and is optically transparent.

A schematic of the test facility is shown in Figure 1. It consists of a primary closed stainless steel piping flow circuit charged with HFE7000 as the working fluid and an instrumented transparent test section for measurement and observation of convective boiling. The secondary flow loop circulates chilled water to condense the working fluid. HFE7000 was chosen as the working fluid due to its low boiling point (34℃) which allows for low gauge pressure test conditions with an operating temperature that is reasonably low. Since the test section is exposed, the low operating temperature reduces heat losses to the environment.

The working fluid is circulated with a gear pump and is then routed to the electric pre-heater, the test section and the condenser sections. As depicted in Figure 1, the working fluid flows through a filter/dryer before it enters the gear pump. The pump circuit is coupled to a 3-phase variable speed motor to control the mass flux. The volumetric flow rate is then measured by a Titan Instruments 945turbine flowmeter with an accuracy within ±3%.
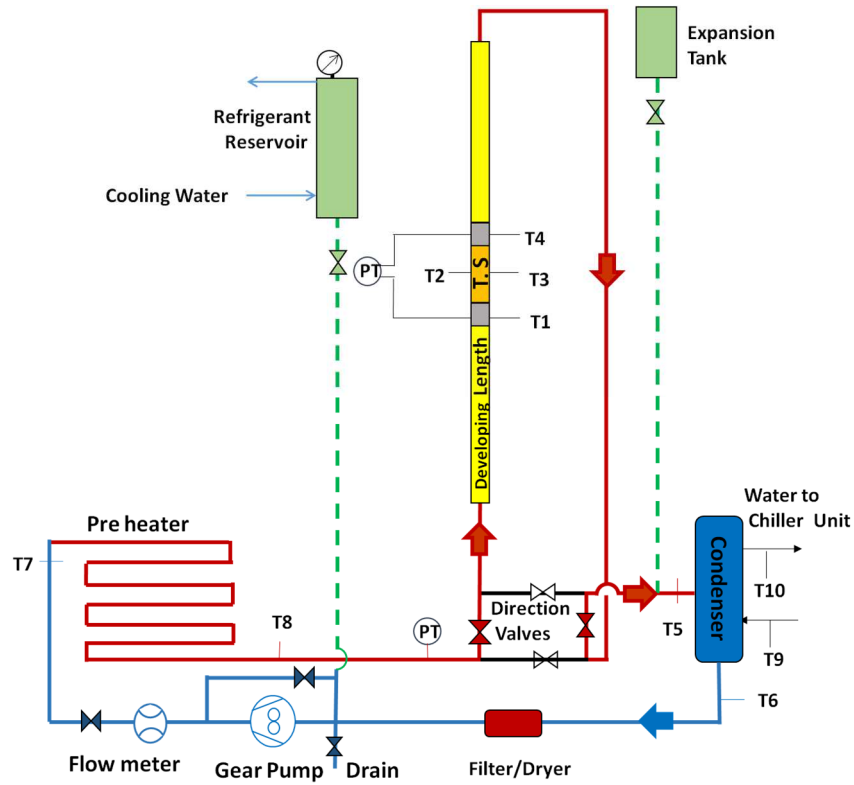
Figure 1: Schematic representation of the rig.

Before entering the vertical test section the working fluid flows through an ohmically heated serpentine stainless steel pre-heater section. The working fluid is heated to the desired thermodynamic state by resistive heating of the stainless steel piping which is sufficiently insulated that losses are negligible. Power was supplied to the preheater with a DC voltage supply. The preheater is of sufficient length that the desired heat transfer to the working fluid can be achieved at moderate heat flux, well below the critical heat flux, and is connected to the main flow loop with dielectric fittings to ensure electrical isolation. The inlet subcooling was controlled

Upon exiting the pre-heater the working fluid is routed to the test section where it is forced upward through a 400 mm long developing length of 8 mm ID glass tubing before entering the main heated test section. The test section depicted in Figure 2 is a 120 mm long transparent tube of 10 mm OD and 8 mm ID. The PEEK connection between the glass tube and the sapphire test section tube was designed carefully to ensure seamless transition so that the flow enters as hydraulically fully developed. It also allows for instrumentation of a thermocouple and pressure port in order to measure the thermodynamic state of the fluid entering the heated test section. Pressure was measured with an Omega PX2401 pressure gauge with an accuracy of ±0.5 kPa.

The outer surface of the sapphire was coated with a 600 nm of ITO, which was sufficient to allow for resistive heating of the outer tube wall at reasonable voltages and currents. A Elektro-Automatik PS8000T DC power supply was connected to the ITO with copper ring electrodes and electrically conductive paste. In this way the test section allowed for visual observation of the flow boiling directly on the diabatic section where it was occurring. The local tube wall temperature at the midpoint of the tube is measured by two diametrically opposed 0.5 mm diameter sheathed T-type thermocouples inserted into drilled wells in the sapphire wall. As will be discussed, the addition of imbedded thermocouples in the sapphire tube allows for the simultaneous measurement of the local heat transfer coefficient, allowing the flow regimes and heat transfer effectiveness to be tracked simultaneously. To facilitate high speed imaging of the two-phase flow a NAC HotShot 1280 high-speed video camera was used. Images were recorded at 1000 fps with a pixel resolution of 1024 x 612.

Upon exiting the test section, the working fluid continues flowing upward through another 400 mm length of glass tube, identical to the lower developing length section and connected with the identical bespoke PEEK fitting. At the top of the test section the refrigerant exits the glass tube through another bespoke PEEK fitting that is machined with an exit port at a 135º angle to reduce the elbow pressure effect that would occur with an abrupt right angle fitting.

Before entering the pump, the two-phase working fluid is condensed in a compact plate heat exchanger cooled by cold water from a temperature controlled precision chiller unit.

The data acquisition system consisted of two National Instruments Compact DAQ 9172 units with several types of module used depending on the measurement taken. Two NI9219 modules were used for the embedded test section thermocouples. Seven NI9211 thermocouple modules were used for the remainder of the thermocouples. The system calibration of these thermocouples was ±0.1°C over the range of temperatures tested. Two NI9215 modules with an accuracy of ±0.03V were used for the high level analogue signals such as pressure, flow meter output etc.

The parameters required to calculate the local heat transfer coefficient are the saturation temperature of the refrigerant (T_{sat}), the tube wall temperature (T_{wall}) and the surface heat flux at the inner wall. With the electrical heating set an approximately constant heat flux is imposed at each point on the tube surface. Thus, knowing the supply voltage potential difference (V) and the current (I) through the ITO coating, the total heat transfer can be calculated simply as:
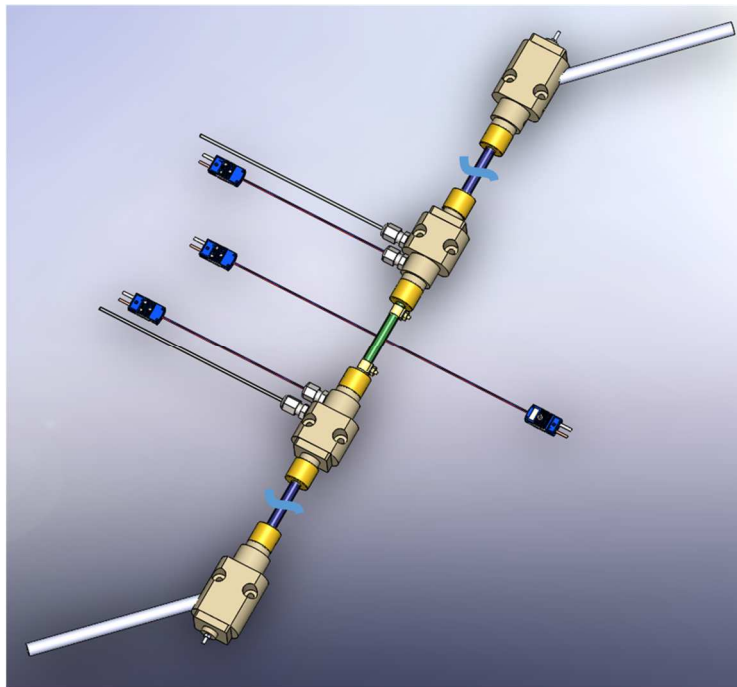
$$q_{add} = V \times I \qquad (1)$$

Figure 2: CAD illustration of the tests section.

In order to determine the quantity of heat transferred to the refrigerant, the heat loss between the external surface and the ambient air has to be subtracted from the heat, supplied;

$$q = q_{add} - q_{loss} \qquad (2)$$

4

The heat loss consists of natural convection, and to a lesser extent radiation, to the ambient surroundings. To quantify the heat losses an experiment was conducted to obtain the value of the effective convection-radiation heat transfer coefficient (h_o). The system was evacuated so that heat transfer was only to the ambient and the test section incrementally heated and a simple correlation for h_o could be estimated from the resulting heat flux – temperature difference curve. In this way, the heat losses during boiling experiments can be estimated through the expression,

$$q_{loss} = h_o A_o (T_{wall} - T_\infty) \tag{3}$$

where T_w-T_∞ is the wall to ambient temperature difference and A_o is the tube outer surface area.

Based on the above, the heat flux to the refrigerant can be estimated as:

$$q^{"} = \frac{VI - h_o A_o (T_w - T_\infty)}{A_i} \tag{4}$$

where A_i is the inner surface area. Thus, the boiling heat transfer coefficient can be estimated as follow:

$$h = \frac{q^{"}}{\Delta T_{sat}} \tag{5}$$

where ΔT_{sat} is the wall superheat T_w-T_{sat}. Here it is appropriate to use T_{sat}, measured at the test section outlet, as the heat sink temperature since the measurement is taken at the mid-point of the heated test section where, for boiling conditions, the fluid is no longer subcooled.

The vapour quality is an important parameter in prescribing the mechanisms of heat transfer for convective boiling, as is evidenced by the fact that it is a parameter used in many predictive correlations for the heat transfer coefficient. It is also a fundamental parameter used in predicting the flow regimes using established flow regime maps.

An energy balance on the heated test section is given as;

$$VI = \dot{m}_{ref} C_p (\Delta T_{sub}) + \dot{m}_{refr} x h_{fg} + q_{loss} \tag{6}$$

The expression illustrates that a portion of the electrical heat supplied to the ITO coating is transferred to the working fluid and some is lost to the ambient surroundings. The portion of the heat transferred to the working fluid can be segmented into that which increases the sensible heat of the slightly subcooled (2K) inlet liquid to saturation after which the heat is converted to latent heat by increasing the vapour quality. Rearranging the above expression, the thermodynamic vapour quality at the exit can be determined as;

$$x_t = \frac{VI - q_{loss} - \dot{m}_{refr} C_p (\Delta T_{sub})}{\dot{m}_{refr} h_{fg}} \tag{7}$$

The uncertainty on derived parameters was calculated using the method of Kline and McClintock [14]. Table 1 lists the measurement uncertainty of the primary measurement whereas Table 2 lists the uncertainty on relevant derived parameters. The uncertainty on the heat transfer coefficient depends on the applied heat flux due to increasing wall superheat with increasing heat flux. Table 2 shows that this uncertainty can be as high as 15% at low applied heat fluxes but decreases monotonically to as low as 3% at the highest applied heat flux.

Table 1: Uncertainty of measured variables.

Parameter	Error
Temperature	$\pm 0.1^0C$

Refrigerant flow rate	±3.0 %
Refrigerant Pressure	±0.5 kPa
Applied High Voltage	±0.05%
Heater Voltage	±0.2%
Heater Current	±0.2%

Table 2: Maximum experimental uncertainties.

Parameter	Maximum Percentage Error
Heat Transfer (W)	± 3 %
Quality	± 5 %
Heat Transfer Coefficient (W/m^{2}K)	± 15% (max) ± 3% (min)

3. Results and Discussion

Visualization of flow regimes under diabatic conditions is not common in the published literature. To the best of knowledge this is one of the first studies to visualize diabatic vertical upward flow boiling, supplementing earlier work by Narcy et al. [15] who used a similar technique to investigate terrestrial and micro-gravity flow boiling. This considered, the first objective of the present work is to investigate the boiling heat transfer in relation to the observed flow regimes.

3.1 Flow Regimes

For the range of mass and heat fluxes tested, three main two-phase flow patterns have been observed bubbly flow, bubbly-slug flow and churn flow. Heretofore, the bubbly-slug flow regime will be referred to as slug flow where it is understood that, in contrast to its adiabatic counterpart, this diabatic scenario involves the formation of slugs which coexist with bubbles in the core flow.

Identifying flow regimes is somewhat subjective. In this study it is complicated by the fact there is significant nucleate boiling on the tube wall which obscures the central region of the flow, which is not the case for adiabatic flow visualization viewing sections. For this study the following was used to identify the various flow regimes.

Bubbly Flow: Bubbly flow was identified as the flow pattern where discrete bubbles occupied the flow region, including the core of the flow. This could include regions where some bubble coalescence has occurred, but the resulting coalesced bubble is still the structure of a bubble.

Slug Flow: Slug flow was identified by the existence of large vapour structures that were of the approximate size of half the tube diameter or larger and were not spherical. Slugs were considered as discrete vapour structures and the flow was still predominantly vertically directed.

Churn Flow: Churn flow was identified by a vapour core that did not contain structured discrete slugs. The flow included horizontal motion (transverse to the flow direction) and chaotic mixing of the phases.

Figure 3 shows the influence of heat flux on the two-phase flow for a fixed mass flux of 100 kg/m^{2}s. Since it is difficult to interpret the flow regimes from still images, Figure 4 is included to give cartoon impressions of the flow regimes based on the high-speed video footage. Figure 3(a) shows the flow regime just following the Onset of Nucleate Boiling (ONB), where it is clear that it is the bubbly flow regime as is to be expected. At this lower heat flux (~9 kW/m^{2}K) the flow regime is bubbly over the entire test section. Increasing the heat flux to ~20 kW/m^{2}K (Figure 3(b)) shows a notable change in the two-phase flow, with a significantly higher bubble density. Regardless the flow regime is still bubbly flow over the whole test section. At ~36 kW/m^{2}K, Figure 3(c) shows that that the flow regime is no longer consistent across the entire test section. Although the lower section is still in the bubbly flow regime, vapour slugs have formed in the core flow of the upper section, with the bubbly-slug flow transition occurring about mid-way along the channel. Near the exit, the flow regime is transitioning to churn flow. Increasing the heat flux to 51 kW/m^{2}K (Figure 3(c)) causes the bubbly-slug transition to occur closer to the channel inlet as well as increasing the size of the slugs in the mid-region of the channel. The slug-churn flow transition is observed to occur lower in the tube. At the highest heat flux (~62 kW/m^{2}K), shown in Figure 3(d), the flow in the upper half of the channel has transitioned to churn flow, as characterized by a core with significant void and vigorous mixing of the phases. Here, slug flow occurs almost immediately at the entrance of the heated test section.
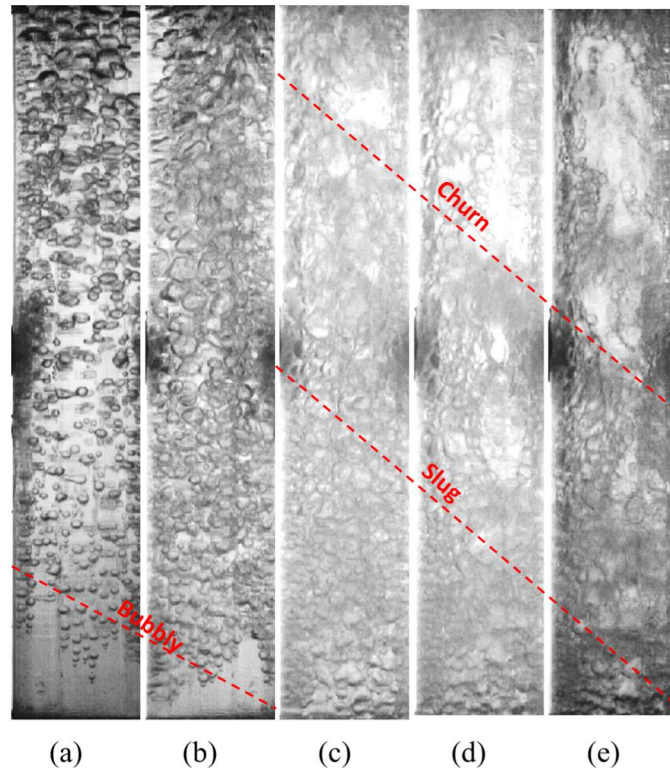

Figure 3: Flow visualisation at 100 kg/m^2 s and different heat flux (a) 8.8 (kW/m^2) (b) 20.3 (kW/m^2) (c) 35.7 (kW/m^2) (d) 51.4 (kW/m^2) (e) 61.7 (kW/m^2).
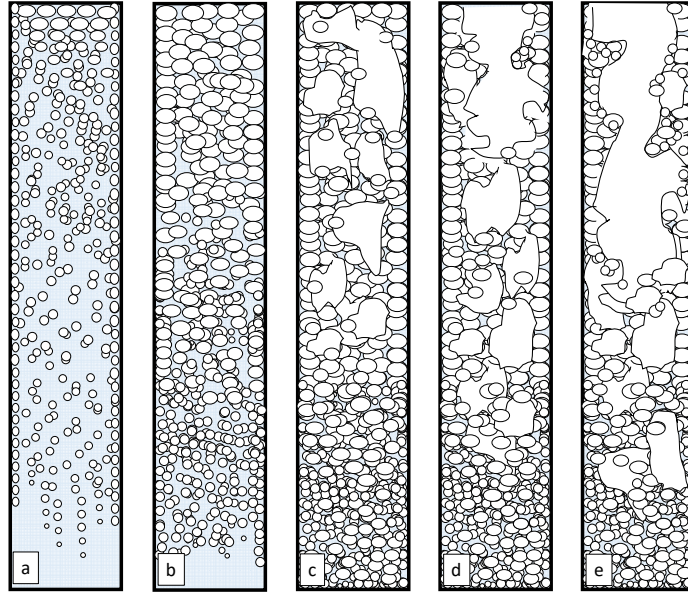
Figure 4: Flow regime cartoons. Considering the midpoint along the tube the flow regimes are (a) partial nucleate boiling: bubbly flow (b) fully developed bubbly flow (c) slug flow (d) slug flow (e) churn flow.

To illustrate the influence of mass flux, Figure 5 shows a comparison between the lowest (50 kg/m^{2}s) and highest (150 kg/m^{2}s) mass fluxes used for this investigation under the same heat flux of ~36 kW/m^2. At the lowest mass flux of 50 kg/m^{2}s the flow regime is bubbly near the entrance, slug in the mid region and churn flow at the top section of the tube (see Figure 5(a)). For the 150 kg/m^{2}s the bubbly-slug flow transition occurs higher up in the tube and churn flow does not appear in the upper region (see Figure 5(b)). Thus, the general effect of increasing mass flux for the same inlet thermodynamic state and applied heat flux is to delay the transition between bubbly-slug and slug-churn flow.

Since the fluid is ostensibly saturated, the heat transferred to the working fluid is converted to latent heat due to the liquid-vapour phase change process. The thermal power, which is the same for the cases considered in Figure 5, thus acts to increase the mixture enthalpy from the inlet to outlet of the test section. Therefore, although the thermal loads are the same, the mixture enthalpy as well as the quality and void fraction at the tube exit decreases with increasing mass flux. Conversely, for the cases considered in Figure 3, where the mass flux is constant and the heat flux is increased, the mixture enthalpy, quality and void fraction at the exit increases. Thus, the influence of the heat and mass flux on the flow regime are related to the thermodynamic state of the two phase mixture and how it influences the local fractions of vapour and liquid that occupy the tube. If a parameter is varied in such a way as to change the exit quality and related void fraction, flow regime transition at a given location along the tube could be influenced.

The thermodynamic state of the two-phase mixture as defined by the mixture enthalpy and quality are not sufficient to pinpoint the flow regime. Depending on the mass flux and heat flux it is possible, for example, to have the same quality yet different flow regimes. Another key element to the established flow regime and flow regime transitions is the bubble dynamics. Since this test facility affords the opportunity to observe the two-phase flow under diabatic conditions i.e. where boiling at the solid-liquid boundary is occurring, some comment is warranted with regard to the phase interactions and their influence on the flow regimes under varying heat and mass flux loadings.

Figure 3(a) shows a clear example of a low heat flux bubbly flow. Here the bubbles nucleate, grow and detach at the heated wall, with some sliding along the wall and some entering the core of the flow. In the lower region the bubbles remain isolated, though moving upward the bubble density increases and some bubble coalescence is observed. As the heat flux increases for a fixed mass flux, Figure 3(b) shows that more nucleation sites have become active. This, together with the observation from the videos that the bubble frequency and departure size also increase, results in more notable bubble coalescence in the core of the flow, though the flow regime

is still bubbly. With further increase in heat flux, the vapour generation rate increases to the extent that the coalescence phenomenon leads to the formation of vapour slugs, though there is still significant nucleate boiling at the tube wall. This is identified here as a bubbly-slug flow regime. Though this is difficult to identify with the still image due to the high density of bubbles near the wall, the slugs are identifiable from the high speed images and are illustrated in the associated cartoon for clarity (See Figures 4). Churn flow occurs when the heat flux and vapour generation rate is high enough to destabilize and/or merge the slugs, causing them to break apart resulting in a chaotic flow regime with rigorous mixing and stirring of the phases. As above, these are difficult to identify with still image so the cartoon in Figure 4 is included as impressions from the high speed video. The high vapour generation rate associated with the higher heat flux results in a significant portion of the core being occupied by vapour.

Figure 5 shows an example of the mass flux influence, here for the lowest and highest mass flux tested for the same heat loading. The still image of Figure 5(b) shows a flow with high bubble density with the flow regime being primarily bubbly, though some slugs are observed to form near the exit region. Compared with the flow of Figure 5(a), the bubbles generated in Figure 5(b) detached from the wall are observed to move faster along the channel due to the higher flow rate. The higher vertical velocity of the bubbles reduces their residency time in the test section and tends to reduce the occurrence of bubble coalescence events so that there is a uniform distribution of small bubbles in the core of the flow. This results in a bubbly flow regime along most of the tube. On the other hand, for the lowest mass flux shown in Figure 5(a), the slower moving bubbles interact with one another and tend to coalesces and form initially larger bubbles which, as the quality continues to increase along the tube length, coalesce to form slugs. Here the slug flow regime begins below the midpoint along the tube. Further along, these slugs merge which opens the core of the flow to high velocity vapour causing aggressive phase interaction resulting in churn flow at the tube exit.
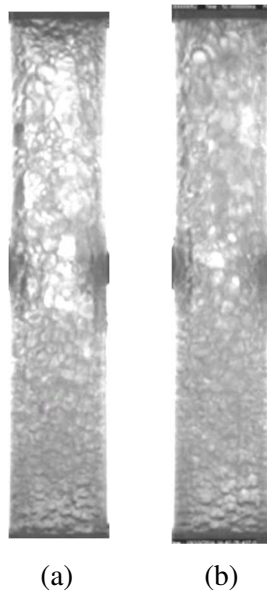

(a)　　　　(b)

Figure 5: Flow visualisation at q''=36 kW/m^2 for different mass fluxes (a) 50 kg/m^{2}s (b) 150 kg/m^{2}s.

3.2 Influence of Heat Flux

A boiling curve plots the imposed wall heat flux versus the superheat of the heated wall and is depicted in Figure 7(a) for the mass flux of 100 kg/m^{2}s. Here the boiling curve is that associated with the midpoint along the test section where the thermocouples are imbedded in the tube wall. The visualization of the flow for this boiling curve is given in Figure 3.

As Figure 6 shows, there are three distinct regions identified by the slope of the q'' vs ΔT_{sup} curve together with visual observations from the high speed video footage. At the low heat flux levels, under slightly subcooled conditions, the mechanism of heat transfer is single-phase forced convection, identified in Figure 6(a) as

Region 1. Increasing the heat flux results in substantial increase in the wall superheat until it is sufficient to initiate bubble nucleation at the ONB and the system enters the bubbly flow regime, shown as Region 2 on the boiling curve. The associated flow image is given in Figure 3(a) which is the bubbly flow regime that occurs just subsequent to ONB. At the previous heat flux setting the flow was single phase until, at the ONB heat flux, one or more nucleation events occurred which subsequently populate most of the surface with active sites. It is an extremely rapid event and is believed to be due to one or more nucleation sites activating which seed neighbouring sites resulting in the cascading sequence of nucleation site seeding until the surface is covered.

Figure 6(a) shows that the initiation of nucleate boiling causes the heated surface temperature to drop significantly as the surface becomes highly populated with nucleation sites. This reduction in superheat shows clear evidence of the enhanced heat transfer mechanisms associated with the presence of the bubbles. Notably, the superheat decreases significantly once nucleate boiling commences indicating a much higher heat transfer coefficient for bubbly flow (Region 2) compared with single phase flow. With further increase in the heat flux the vapour generation rate is high enough to cause bubble coalescence in the core of the flow and the flow transitions to the slug flow regime, as described in the last section. With regard to the heat transfer, the boiling curve shows a change in slope when this flow regime transition occurs signifying a change in the mechanisms of heat transfer in Region 3, which here is improved over that of the bubbly flow regime. Entering the churn flow regime (Region 4) does not show as significant change in the slope of the boiling curve.

An interesting observation here is that the bubbly-slug flow transition coincides with a change in the measured heat transfer characteristics. This mirrors what is observed from the boiling curve after the ONB where the single-phase to nucleate boiling flow regime transition occurs. This is of course a novelty of this test section where the local heat transfer and flow regimes can be considered together. The implication is that bubbly-slug flow transition can be pinpointed in a more quantitative manner compared with solely visual observation, which involves a level of subjectivity and requires a transparent and diabatic test section.

Figure 7 plots the heat transfer coefficient with respect to increasing heat flux. Initially, the figure shows a constant heat transfer coefficient with the increase of heat flux up to about 9 kW/m^2, and this is representative of single phase liquid flow prior to ONB (Region 1). The constant heat transfer coefficient trend is expected for hydrodynamically developed single-phase flow as it primarily depends on the Reynolds number. An sensitivity to heat flux and changes in fluid property variations with temperature are within the experimental uncertainty of these experiments.

Figure 7 shows the dramatic increase of heat transfer coefficient subsequent to the ONB and the beginning of the bubbly flow regime (Region 2), as it increases by over 400% subsequent to the ONB. The difference in measured wall superheat between just prior to and just subsequent to boiling incipience is known as the temperature overshoot. In this experiment the overshoot was about 22 ºC, which is large due to the relatively smooth sapphire surface and the highly wetting properties of HFE 7000 which tends to flood potential nucleation sites. It should be noted that when the heat flux was incrementally lowered, nucleate boiling could be maintained down to wall superheats as low as 1K, illustrating the boiling hysteresis effect.
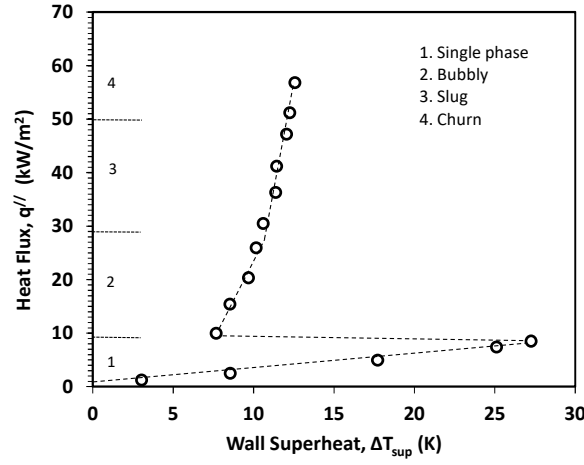
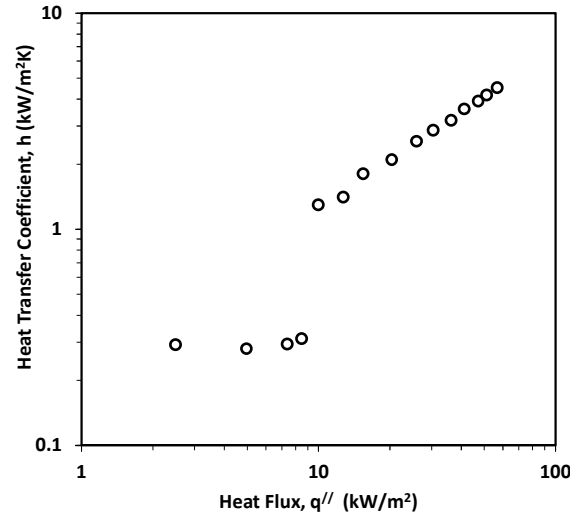**Figure 6**: Boiling curve for 100 kg/m²s, ΔT_{sub}=2 K.

Figure 7: Heat transfer coefficient versus heat flux for 100 kg/m²s, ΔT_{sub}=2 K.

Increasing the heat flux beyond the ONB, the high-speed videos show that continuously more nucleation sites are activated (Figure 3(a) to (e)) and the bubble frequency and departure size increase. Compared to single phase flow, where the increase in heat flux increases the sensible heat of the liquid phase, here the increased heat flux increases the vapour generation rate and the local quality. As Figure 6 shows, compared with single phase flow, only small increases in the wall superheat occur for like increases in heat flux (Region 2). Also, Figure 7 shows that subsequent to the ONB the heat transfer coefficient increases with increasing heat flux indicating that the heat transfer mechanisms improve with increase in the vapour generation rate, signifying that the increase in the bubble activity and phase interaction is responsible for escalating the heat transfer coefficient, and this is qualitatively consistent with the observation made from the high speed videos. After ONB the heat transfer coefficient increases with a power law of $h \propto (q'')^{2.8}$. This cubic relationship illustrates that the presence of the bubbles improves the effectiveness of the heat transfer, with higher vapour generation rates resulting in higher heat transfer coefficients.

3.3 Influence of Mass Flux

Figure 8 shows the heat transfer coefficient for the three mass fluxes tested. It is clear that the heat transfer coefficient is insensitive to the mass flux. This suggests that, for the low mass fluxes tested, the dominant heat

transfer mechanisms are associated with the local bubble activity and phase interactions opposed to convective influences, which is consistent with earlier convective boiling studies [16-18]. However, considering the boiling curves shown in Figure 9, there are some subtle differences between the different mass fluxes. As discussed earlier, the magnitude of the mass flux influences the local flow regime, with increasing mass flux tending to delay flow regime transition. This is clear in Figure 9 where the elbow in the boiling curve, which corresponds with the observed transition from bubbly to slug flow, occurs at higher heat fluxes as the mass flux is increased. Although not immediately discernible from the boiling curves, the slug-churn flow transition heat flux also increases with increasing mass flow rate. The key observation here is that, for a given heat flux, the mass flux influences the local flow regime, in part by influencing the bubble dynamics, and in part by influencing the thermodynamic quality and related void fraction. With regard to quality and void fraction, increasing the mass flux for a fixed heat flux acts to decrease the quality and void fraction and this of course influences the flow regime. However, considering the bubbly-slug flow transition at the measurement location, the quality associated with the transition heat flux decreases from $x \sim 5\%$ at 50 kg/m^{2}s to $x \sim 1.5\%$ at 150 kg/m^{2}s. Although many void-quality models are available, for the purpose of the present analysis where one is more interested on macroscopic trends opposed to rigorous accuracy, the void fraction can be estimated using the momentum flux model as;

$$\alpha = \frac{1}{1 + \frac{1-x}{x}\left(\frac{\rho_g}{\rho_l}\right)^{2/3}} \tag{8}$$

such that the estimated void fraction at the bubbly-slug transition heat flux decreases from $\alpha \sim 65\%$ at 50 kg/m^{2}s to $\alpha \sim 35\%$ at 150 kg/m^{2}s. This illustrates that it seems that there is not a critical vapour fraction quantity that defines flow regime transition and that bubble dynamics and phase interactions also play an important role. Regardless, for the relatively low mass fluxes tested here, it is clear that bubbly-slug and slug-churn flow transition occurs at notably higher vapour fractions (quality and void fraction) for lower mass fluxes.
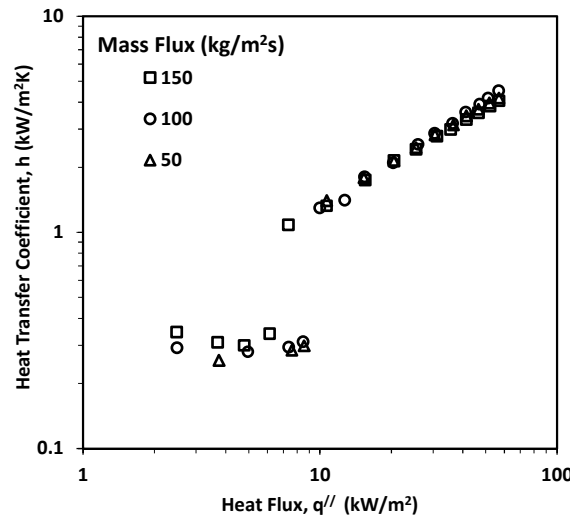

Figure 8: Heat transfer coefficient versus heat flux for different mass fluxes.
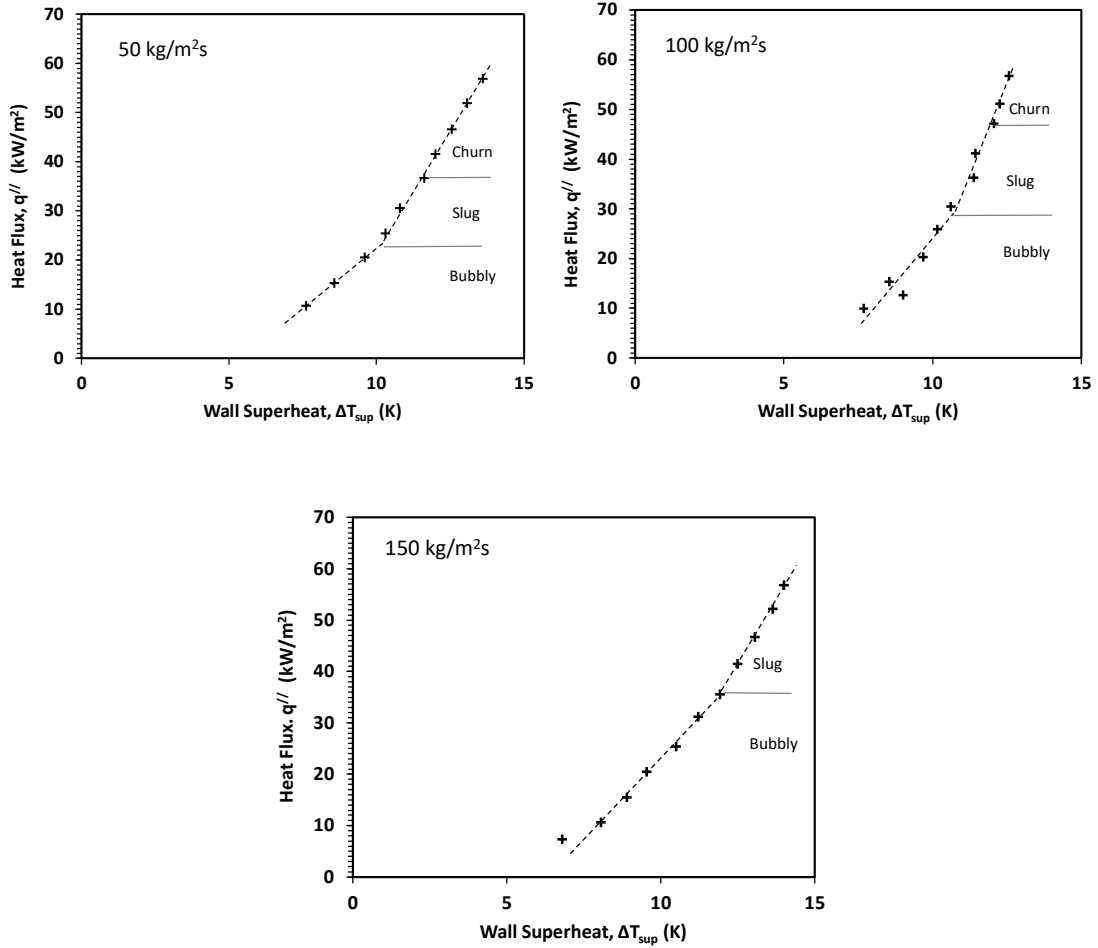
Figure 9: Boiling curves for different mass fluxes, (Top) 50 kg/m²s, (Middle) 100 kg/m²s (Bottom) 150 kg/m²s.

4. Revisiting the Chen Correlation

Several correlations have been proposed to predict the heat transfer coefficient for convective flow boiling. A subset of these are applicable to the current case of vertical upflow boiling. However, the intention here is not to provide an exhaustive evaluation of these different correlations. However, it seems appropriate to summarize some finding, in particular with respect to the Chen [3] correlation due to its widespread use in the literature as well as in industry.

Chen [3] was one of the first to propose a robust correlation for convective boiling and it, along with many modified versions of it, have been used to predict the convective boiling heat transfer coefficient for over half a century. It is, without doubt, the most cited correlation for convective boiling heat transfer and it seems prudent to revisit this work in the context of the present measurements, since it is rare to have local heat transfer and flow regimes to consider together. In particular, the Chen correlation was based on mechanistic sub-models opposed to brute-force regression analysis. With the new data one can, to some extent, evaluate the applicability of the mechanistic sub-models and associated assumptions in the context of the observed flow regimes and heat transfer.

Chen [3] proposed a method whereby convective boiling heat transfer is a function of both bulk convection and nucleate boiling mechanisms, with the latter accounting for the nucleation and growth of bubbles. These represented what was termed macroconvection and microconvection heat transfer mechanisms respectively. The core postulate was that in forced convective boiling, the mechanisms of both bulk convection and nucleate boiling would be modified from their base mechanisms (i.e. single phase forced convection and nucleate pool boiling) due to the effects of non-zero vapour quality. Furthermore, the macro and micro convection mechanisms would be interdependent, in that the two mechanisms would interact with one another. Finally, Chen assumed that the two heat transfer mechanisms could be superimposed such that,

$$h_{TP} = h_{macro} + h_{micro} \qquad (9)$$

The superimposition of the two mechanisms to formulate an effective two-phase heat transfer coefficient was somewhat *ad hoc*, in that it was justified on the basis that some previous studies had done so. However, from a thermal network perspective, an alternative interpretation can be given based on the premise that the two mechanisms are acting simultaneously to transport heat from the heated surface. The additive assumption thus represents that the two mechanisms are acting thermally in parallel. One can argue that, from a time-averaged point of view, this assumption is reasonable as it states that at any given location, both bulk convection and microconvetion effects determine the effectiveness of the heat transfer.

The macroconvection was postulated to be predictable with a Dittus-Boelter type correlation for a vapour-liquid mixture with effective properties that are related to the relative vapour fraction,

$$h_{macro} = 0.023(FRe_l^{0.8})Pr_l^{0.4}\frac{k_l}{D} \qquad (10)$$

where the Reynolds number factor, F, represents a ratio of the two-phase Reynolds number to the liquid Reynolds number, $F=(Re_{TP}/Re_l)^{0.8}$, with the liquid Reynolds number being based on the liquid fraction of the flow,

$$Re_l = \frac{(1-x)GD}{\mu_l} \qquad (11)$$

Thus, the factor F is strictly a flow parameter introduced such that the Reynolds number in the Dittus-Boelter equation represents that of the two-phase mixture. Chen then drew the analogy with momentum transfer such that F was related to the Martinelli parameter,

$$X_{tt} = \left(\frac{1-x}{x}\right)^{0.9}\left(\frac{\rho_g}{\rho_l}\right)^{0.5}\left(\frac{\mu_l}{\mu_g}\right)^{0.1} \qquad (12)$$

Albeit a graphical solution at the time, subsequent researchers have correlated the parameter in order that it is more convenient to use. Chen and Fang [19] revisited the Chen correlation and provided an assessment of various correlating functions for F and suggested the following be used;

$$F = \begin{cases} 2.35\left(\frac{1}{X_{tt}} + 0.213\right)^{0.736} & if \ \frac{1}{X_{tt}} > 0.1 \\ 1 & if \ \frac{1}{X_{tt}} \le 0.1 \end{cases} \qquad (13)$$

The microconvection component of the two-phase heat transfer coefficient was hypothesized as being induced by the agitation caused by the bubbles nucleating and growing at the wall. To facilitate this mathematically, Chen used the Forster and Zuber [20] pool boiling model. The main Forster and Zuber postulate was that the microconvection induced by growing bubbles was mechanistic and related to the bubble size and growth rate, which could be estimated analytically from the extended Rayleigh equation. This provided length and velocity scales that could be used to define an effective Reynolds number that was subsequently implemented in a typical power law relation of the form $Nu_b=CRe_b^nPr^m$.

A key assumption of the Forster and Zuber analysis was that the agitation responsible for the microconvection during boiling was related to the size and growth rate of the growing bubbles. Analytically, bubble growth was approximated as being diffusion controlled and of the scale of that for spherical bubble growth in a uniformly superheated liquid commensurate with the wall superheat. As noted by Chen, this assumption is plausible if bubble growth occurs within a thermal boundary layer which is quite thick compared with the size of the bubbles. These assumptions led to the result whereby, for a given superheat, the product of the instantaneous bubble radius, R, and the expansion growth rate, dR/dt, is constant. This stems from the fact that diffusion-controlled bubble growth is governed by heat conduction with a fixed superheat across a thermal boundary layer that grows as $\delta \sim {}^1\!/_3(\alpha t)^{1/2}$ such that $dR/dt \sim t^{-1/2}$ and $R \sim t^{1/2}$ [21]. In the context of the microconvection Reynolds number, the result is that it is constant since $R(dR/dt)$ is constant i.e. the increased radius during bubble growth is exactly compensated by a reduced growth rate such that the overall scale of the liquid agitation remains constant. Subsequent to the development of this mechanistic sub-model, the analysis becomes empirical whereby the leading coefficient and exponents in the Nusselt number power law relation are determined from fitting experimental boiling data.

Chen coupled the macroconvection with the microconvection by postulating that the bulk flow had the effect of thinning the thermal boundary layer, compared with that of pool boiling, to such an extent that it could no longer be assumed that the scale of the bubble expansion rate was that of a uniform superheat. The steeper thermal gradients within the thinned thermal boundary layer results in the bubble being exposed to continually lower superheat as it expands, which should reduce its growth rate with a subsequent diminishing influence on the liquid agitation and microconvection Reynolds number. To account for this influence, Chen applied a suppression factor multiplier, S, to the Forster and Zuber semi-empirical correlation such that;

$$h_{micro} = \left[0.00122 \left(\frac{k_l^{0.79} C_{p.l}^{0.45} \rho_l^{0.49}}{\sigma^{0.5} \mu_l^{0.29} h_{fg}^{024} \rho_g^{0.24}} \right) \Delta T_{sat}^{0.24} \Delta P_{sat}^{0.75} \right] S \quad (14)$$

where S was assumed to be a function of the two phase Reynolds number, $Re_{TP} = Re_l F^{1.25}$, in order to account for the influence of flow rate and vapour quality. In the limits of $Re_{TP} \to 0$, $S \to 1$ and $Re_{TP} \to \infty$, $S \to 0$, the suppression factor was determined empirically, again as a graphical function. Once again, Chen and Fang [19] provided an assessment of various correlating functions for S and suggested the following be used;

$$S = \frac{1}{1 + 2.53 \times 10^{-6} (Re_l F^{1.25})^{1.17}} \quad (15)$$

The predicted and measured convective boiling heat transfer coefficients are compared in Figure 10. The figure shows relatively good agreement, in particular at the lower heat transfer coefficient levels which is associated with lower heat fluxes. Table 3 is included to quantify the level of agreement, where the MARD is the Mean Absolute Relative Deviation and the MRD is the Mean Relative Deviation,

$$MARD = \frac{1}{n} \sum \left| (h_{exp} - h_{pre}) / h_{exp} \right| \times 100\% \quad (16)$$

$$MRD = \frac{1}{n} \sum (h_{exp} - h_{pre}) / h_{exp} \times 100\% \quad (17)$$

Table 3: Comparison between experimental data and correlation predictions.

	MRD	MARD
Chen (1966)	-17%	22%
Chen-Cooper (Present)	-3%	5%

Accordingly, the Chen correlation is seen to generally under predict the measured heat transfer coefficients with a MRD=-17%, with the underprediction getting progressively worse at higher heat fluxes with an overall MAD=22%. It is interesting to note that the Chen correlation provides very reasonable predictions at the lower heat fluxes (generally when $h<2500$ W/m^2K), where bubbly flow is the observed flow regime, which is consistent with the mechanistic sub-model for the microconvection heat transfer. For the higher heat fluxes, the single-phase contribution, h_{macro} in Eq. 9, to the overall heat transfer coefficient, h_{TP}, is only between 5-10%, indicating that it is the accuracy of the boiling microconvection model for h_{micro} that is responsible for the discrepancy. It is also why, for the conditions tested, the Chen prediction is not sensitive to mass flux, which is consistent with these low mass flux measurements.

For the low mass flux cases considered here, the suppression factor, S, is very close to unity. Thus, the influence of the two-phase Reynolds number on the microconvection is relatively unimportant. In the context of the mechanistic sub-model, this says that the thermal boundary layer is not significantly affected by the bulk flow and that the scale of the bubble agitation is commensurate with that of nucleate pool boiling. This can then be considered in the context of the applicability of the Forster and Zuber correlation, which has not proven to be the most accurate pool boiling correlation compared with those which were developed later. In particular, the Cooper [22] correlation has been shown time and again to provide a very good prediction of pool boiling heat transfer [23-25],

$$h_{micro} = 55 P_R^{0.12-0.087 \ln \varepsilon} (-0.4343 ln P_R)^{-0.55} M^{-0.5} q''^{0.67} \quad (18)$$

Since $S \approx 1$, it is possible to directly substitute the Cooper correlation for that of the Forster and Zuber correlation in Eq. 9 without disrupting the fundamental hypothesis of the Chen analysis for the microconvection heat transfer estimation. Furthermore, the empirical factor F was shown by Chen to agree with the basic formulation based on momentum transfer analogy, so is not exclusive to the data set from which the factor was empirically determined. Therefore, applying the factor F to the macroconvection heat transfer estimation is appropriate even if a different pool boiling correlation is used for the microconvection prediction. These being the case, the two-phase heat transfer coefficient has here been estimated in this way where the macroconvection is predicted by Eq. 10 and the microconvection with Eq. 18, using the suggested default roughness of $\varepsilon=1$ μm. The results, shown in Figure 11, give excellent agreement with the present low mass flux measurements, with a MRD=-3% and a MARD=5% (see Table 3).
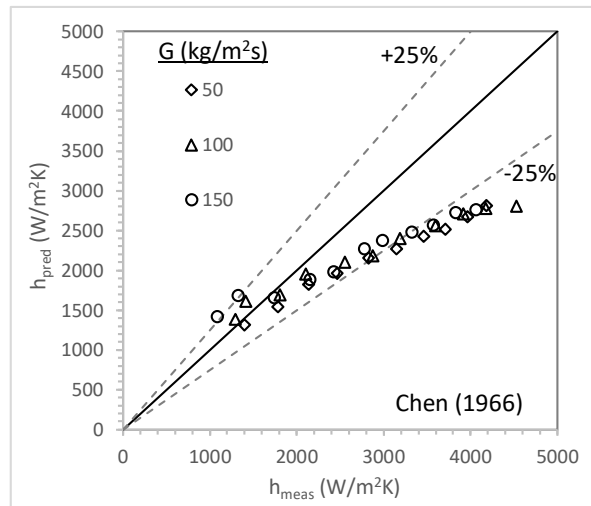

Figure 10: Measured and predicted heat transfer coefficients using the Chen [3] correlation.
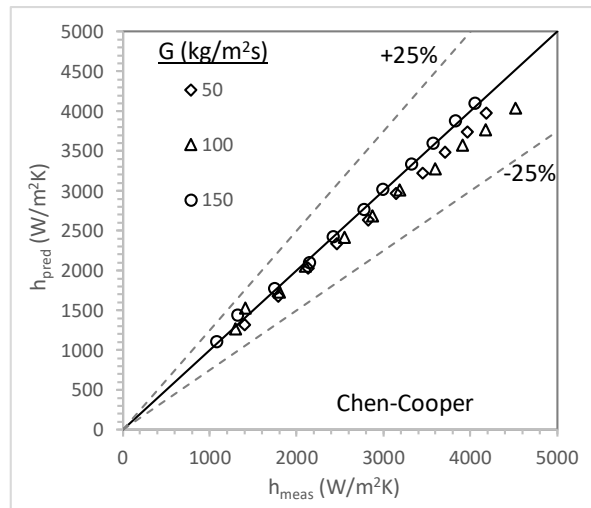
Figure 11: Measured and predicted heat transfer coefficients using the Chen-Cooper modification.

5. Conclusions

An experimental investigation of upward vertical flow boiling of HFE7000 has been performed in a circular heat exchanger. To the best of knowledge this is one of the first studies to obtain local heat transfer data with full visual access to determine the associated flow regime for this flow configuration. Results show that the heat transfer coefficient is a function of imposed heat flux, which is evidence to suggest that the dominant heat transfer mechanisms are associated with the local bubble activity opposed to bulk convective influences. In particular, the boiling dictates the flow regime and an interesting result is that the boiling heat transfer coefficient asymptotically matches a linear line for bubbly flow at lower heat fluxes and a higher slope line at higher heat fluxes for the more rigorous slug and churn flow regimes. The inflection region was observed to occur near the transition from bubbly flow to slug flow. For the range of mass fluxes tested, it was shown that the heat transfer was generally insensitive to mass flux, again indicating that the dominant heat transfer mechanism is associated with boiling. However, the flow regime transitions were found to be delayed with increasing mass flux.

The Chen [3] flow boiling correlation was compared with the measured heat transfer data and showed reasonably good agreement, in particular for the lower heat flux data where the flow regime was bubbly. The correlation did not well predict the churn flow heat transfer measurements. It was found that for the low mass fluxes tested here the suppression factor, used to augment the boiling heat transfer contribution to the overall two-phase heat transfer, was approximately unity for all cases. This allowed the direct substitution of the more accurate Cooper pool boiling correlation to be used in the Chen correlation to quantify the boiling contribution to the overall heat transfer. Doing so resulted in excellent agreement between predicted and experimental data.

Acknowledgements

Nomenclature

A   surface area, m^2
C_p refrigerant specific heat, J/(kg K)
D   test section inner diameter, m
F   convective enhancement factor
G   mass flux, kg/(m^2 s)

h_{fg} latent heat, J/ kg
I   current, A
k   thermal conductivity, W/(m K)
h   heat transfer coefficient W/(m² K)
$\dot{m}$ mass flow rate, kg/s
P   pressure, Pa
Pr   Prandtl number
R_e Reynolds number
R_p average surface roughness, μm
q   heat transfer, W
q_{add} heat added to the outer tube surface, W
q_{loss} heat lost to the ambient, W
q''   heat flux from channel wall to fluid, W/m²
S   suppression factor
T   temperature, K
V   voltage
x   thermodynamic quality
X_{tt} Lockart-Martinelli parameter

Subscipts
exp   experimental
i   inner
g   gas
l   liquid
o   out
macro   macroconvection
micro   microconvection
refr   refrigerant
pre   prediction
sat   saturation
sub   subcooled
TP   two phase
w   wall

Greek symbols
ε   surface roughness, μm
α   void fraction
μ   dynamic viscosity
ρ   density
σ   surface tension, N/m
∞   ambient

References

[1] S.G. Kandlikar, High Flux Heat Removal with Microchannels—A Roadmap of Challenges and Opportunities, Heat Transf. Eng. 26 (8) (2005) 5–14.
[2] J. B. Copetti, M. H. Macagnan, F. Zinani, N.L.F. Kunsler, Flow boiling heat transfer and pressure drop of R-134a in a mini tube: an experimental investigation, Exp. Therm. Fluid Sci. 35 (4) (2011) 636–644.
[3] C. Chen, P. Gao, S. Tan, H. Chen, X. Chen, Forced convective boiling heat transfer of water in vertical rectangular narrow channel, Nucl. Eng. Des. 291 (2015) 133–144.
[4] J. C. Chen, 'Correlation for Boiling Heat Transfer to Saturated Fluids in Convective Flow', Ind. Eng. Chem. Process Des. Dev. 5 (3) (1996) 322–329.

[5] M.M. Shah, A New Correlation for Heat Transfer During Boiling Flow Through Pipes, ASHRAE Trans. 82 (2) (1976) 66-86.

[6] G.M., Lazarek, S.H. Black, Evaporative heat transfer pressure drop and critical heat flux in a small vertical tube with R-113. Int. J. Heat and Mass Transf. 25 (1982) 945-960.

[7] K. E. Gungor, R. H. S. Winterton, A general correlation for flow boiling in tubes and annuli, *Int. J. Heat Mass Transf.* 29 (3) (1986) 351–358.

[8] K. E. Gungor, R. H. S. Winterton, Simplified general correlation for saturated flow boiling and comparisons of correlations with data, Chem. Eng. Res. Des. 65 (2) (1987) 148–156.

[9] D.B.R. Kenning, M.G. Cooper, Saturated flow boiling of water in vertical tubes. Int. J. Heat and Mass Transf. 32 (1989) 445-458.

[10] S.G. Kandlikar, A General Correlation for Saturated Two-Phase Flow Boiling Heat Transfer Inside Horizontal and Vertical Tubes, J. Heat Transf. 112 (1990) 219-228.

[11] Z. Liu, R.H.S. Winterton, A general correlation for saturated and subcooled flow boiling in tubes and annuli based on a nucleate pool boiling equation. Int. J. Heat and Mass Transf. 34 (1991) 2759-2766.

[12] J.P. Wattelet, Predicting boiling heat transfer in a small-diameter round tube using an asymptotic method, in *Convective Flow Boiling*, (1995) 377–382.

[13] L. Sun, K. Mishima, An evaluation of prediction methods for saturated flow boiling heat transfer in mini-channels. Int. J. Heat and Mass Transf. 52 (2009) 5323-5329.

[14] S.J. Kline, F.A McClintock, Describing uncertainties in single sample experiments, Mechanical Engineering 3-8 (1953).

[15] M. Narcy, E. de Malmazet, C. Colin, Flow boiling in tube under normal gravity and microgravity conditions, Int. J. Multiphase Flow 60 (2014) 50–63.

[16] K. Cornwell and P. A. Kew, Boiling in Small Parallel Channels, in Energy Efficiency in Process Technology, Springer, Dordrecht (1993) 624–638.

[17] R. A. Buchanan, T. A. Shedd, Extensive Parametric Study of Heat Transfer to Arrays of Oblique Impinging Jets With Phase Change, J. Heat Transf. 135 (11) (2013) 111017.

[18] R. Jenkins, C. de Brún, T.L. Lupton, R. Lupoi, R. Kempers, A.J. Robinson, Convective Boiling of Confined Impinging Jet Arrays, Exp. Therm. Fluid Sci. 86 (2017) 224-234.

[19] W. Chen, X. Fang, A note on the Chen correlation of saturated flow boiling heat transfer, Int. J. Refrig. 48 (2014) 100–104.

[20] H. K. Forster, N. Zuber, Dynamics of vapor bubbles and boiling heat transfer, AIChE J. 1 (4) (1955) 531–535.

[21] A.J. Robinson, R.L. Judd, The Dynamics of Spherical Bubble Growth, Int. J. Heat Mass Transf. 47 (23) (2004) 5101-5113.

[22] Cooper, M.G. (1984). Heat flow rates in saturated nucleate pool boiling – a wide ranging examination using reduced properties. Adv. Heat Transf. 16 (1984) 157-239.

[23] W-T Ji, C-Y Zhao, Y-L He, W-Q Tao, Experimental validation of Cooper correlation at higher heat flux, Int. J. Heat and Mass Transf. 90 (2015) 1241–1243.

[24] D. Junga, Y. Kim, Y. Ko, K. Song, Nucleate boiling heat transfer coefficients of pure halogenated refrigerants, Int. J. Refrig. 26 (2003) 240–248.

[25] C-B Chiou, D-CLu, C-C Wang, Pool boiling of R-22, R-124 and R-134a on a plain tube, Int. J. Heat Mass Transf. 40 (7) (1997) 1657-1666.